A Light-weight Free-standing Graphene Foam-based Interlayer towards Improved Li-S Cells

Ruowei Yi[a,b], Chenguang Liu[c,d], Yinchao Zhao[c,d], Laurence J. Hardwick[b], Yinqing Li[e], Xianwei Geng[f], Qian Zhang[a,b], Li Yang [a,b*], Cezhou Zhao[c**]

[a] *Department of Chemistry, Xi'an Jiaotong-Liverpool University, Suzhou, Jiangsu 215123, China*

[b] *Stephenson Institute for Renewable Energy, Department of Chemistry, University of Liverpool, Liverpool L69 7ZD, UK*

[c] *Department of Electrical and Electronic Engineering, Xi'an Jiaotong-Liverpool University, Suzhou 215123, China*

[d] *Department of Electrical Engineering and Electronics, University of Liverpool, Liverpool L69 3GJ, UK,*

[e]*Dongguan Hongde Battery Ltd.Co., Dongguan 523649, China*

[f] *School of Materials Science and Engineering, Central South University, Changsha 410083, China*

*Corresponding authors.

**Corresponding authors.

E-mail addresses: li.yang@xjtlu.edu.cn (L. Yang); cezhou.zhao@xjtlu.edu.cn (C. Zhao)

Abstract:

A light-weight and free-standing graphene foam interlayer placed between sulfur cathode and separator is investigated to improve the electrochemical performance of lithium-sulfur batteries. The highly conductive and light-weight porous graphene foam not only increases the electron pathway of cathode, but also adsorbs the dissolved high-order lithium polysulfides during cycles, thus the loss of active materials is greatly avoided with only minimum mass addition approximately 0.3 mg cm^{-2} on cathodic side. Additionally, the atomic layer deposition method is applied to deposit the zinc oxide nano-scale coating on graphene foam interlayer in order to chemically trap the polysulfides with minimized deterioration on conductivity of graphene foam. Among all the graphene foam, graphene foam@zinc oxide and graphene foam/graphene foam@zinc oxide interlayers, the graphene foam/graphene foam@zinc oxide exhibits the best electrochemical performance, delivering an initial specific capacity of 1051 mAh g^{-1} at 0.5 C and retaining a reversible capacity of 672 mAh g^{-1} after 100 cycles, while the cell without interlayer only shows 346 mAh g^{-1}. These results demonstrate the strategy of including a zinc oxide modified graphene foam interlayer as an effective light-weight interlayer for improving Li-S cell performance.

Key words: Li-S battery; Graphene foam; Interlayer; Atomic layer deposition; ZnO

1. Introduction

As one of the most attractive competitors *versus* lithium-ion battery (LIB), Li-S battery attracts much attention due to its high theoretical energy density of 2500 Wh kg^{-1} [1] and specific capacity of 1672 mAh g^{-1} [2] that are about three times of those of LIB [3-5], plus other advantages for example the abundant existence of sulfur on earth and being environmental friendly element [5-8]. Therefore, Li-S battery holds great promises as an alternative for LIB in high power devices like electric vehicles (EV) and hybrid energy vehicles (HEV), which urgently seek for high capacity electric sources [9-11]. However, the insulation nature of elemental sulfur and lithium sulfides [12, 13], the large volumetric expansion of sulfur during lithiation [13, 14], and the dissolution of highly order lithium polysulfides intermediates, known as "shuttle effect" [15-20], still hinder it from large-scale practical applications, and they often result in the low utilization of the active material and severe capacity fading after cycles [21, 22].

Over the past decades, many approaches for addressing these performance-related problems have been extensively developed, and most of them focused on infiltration of sulfur into conductive porous host, including porous carbon materials [23-26] and conductive polymers [27-29]. These porous hosts not only provide enhanced conductivity for sulfur, but also suppress the diffusion of dissolved polysulfides. Besides, some metal oxides have also been employed to further absorb the polysulfides by acting as chemical absorption sites [7, 13, 18, 30, 31]. However, the fabrication processes of these composites are usually complicated [32, 33], meanwhile the

introduction of other materials also decreases the gravimetric sulfur loading of cathode [34]. Consequently, the gravimetric specific capacity of the whole battery is still not satisfactory.

To explore a feasible approach that promotes the performance of Li-S battery without decreasing sulfur loading, one strategy focusing on capturing the polysulfides outside the cathode shows great promises [35]. The multiwall carbon nanotube paper (MWCNT paper) [36] and microporous carbon paper (MCP) [35] are firstly applied as the bifunctional interlayer between separator and cathode, which not only decrease the internal charge transfer resistance but also localize the soluble polysulfides. Following this idea, other materials have been applied as interlayer, including pure nickel foam [37], carbonized paper [38, 39], microporous carbon black [35, 40, 41], carbon nanofibers/nanotubes [10, 36, 42], conductive polymers [43] and so on. These interlayers can effectively immobilize and recycle the dissolved polysulfides, thus moderate the shuttle effect and improve the electrochemical performance of Li-S batteries [44]. Nevertheless, the application of this configuration significantly increases both the thickness and weight of cathode, as these interlayers are usually about dozens to hundreds micrometers in thickness and dozens milligram per square centimeter in density [33, 37, 38, 42, 45], which are close to those of a common sulfur-containing cathode. Consequently, it undermines the overall energy density and offsets the gains in battery performance [46]. Therefore, it is essential to develop a polysulfide-blocking interlayer without much mass and volume addition.

Recent studies have been reported that metal oxides can be effective polysulfides-trappers [47] , including α-Fe_2O_3 [7], MnO_2 [18, 30, 48], TiO_2 [13, 14], Al_2O_3 [6] and ZnO [45, 49, 50]. Among them, ZnO shows strong chemical confining effect of polysulfides due to the Li-O interaction, and its binding energy for Li_2S_8 is one of the highest values among other metal composites [45, 51]. Besides, ZnO has also attracted great attention due to its relative stability, low cost and environmental friendliness [50]. However, these metal oxides are usually electrically insulating, it is essential to minimize their loadings in order to avoid the increase of impedance and the decline in the overall gravimetric capacity and energy density [52]. Therefore, it is desirable to effectively enhance the conductivity while keeping the abilities of trapping the polysulfides. With such a target in mind, we propose to incorporate graphene with metal oxides. Graphene, since its experimental discovery in 2004, has already been foreseen as an important future technology. This carbon monolayer exhibits superior electrical conductivity, high specific surface area and good structural stability, which has been widely used to ameliorate the challenges of the Li-S system [53, 54].

Herein, a free-standing graphene foam (GF) interlayer has been applied as an interlayer between S-C cathode and separator. The highly conductive light-weight graphene foam not only provides effective remission for electrode polarization, but also keeps the weight addition to be less than 5 wt. %, thus minimizing the decrease of whole energy density. To further enhance its polysulfide-blocking ability, the atomic layer deposition (ALD) method is used to deposit a nanoscale ZnO coating on GF interlayer

(GF@ZnO) in order to minimize the deterioration on conductivity [16, 52]. With this modified separator, a sulfur cathode prepared by commercial elemental sulfur with 60 wt. % sulfur loading, reveals a high initial reversible capacity of 1051 mAh g^{-1} at 0.5 C, with a cycle decay value of 0.36% per cycle. These fundamental studies suggest that this light-weight free-standing graphene foam interlayer has potential for next generation high performance lithium−sulfur batteries.

2. Experimental section

Synthesis of GF

Nickel foams (Liyuan Novel Materials from Changde (China), ~ 320 g m^{-2} in area density and ~ 1 mm in thickness) were used as three-dimensional (3D) scaffold templates for the chemical vapour deposition (CVD) growth of GF [55]. Typically, 35×35 mm^2 of nickel foam pieces were firstly rolled to 0.3 mm thickness and heated to 1000 °C at 10 °C min^{-1} under a mixed flow of Ar (1000 s.c.c.m) and H_2 (500 s.c.c.m) in a tube furnace, and annealed for 5 min. Then a CH_4 flow of 50 s.c.c.m was introduced into the reaction tube. After 5 min of reaction-gas mixture flow, the CH_4 was turned off and samples were rapidly cooled down to room temperature at a rate of ~ 100 °C min^{-1}. Then the samples were etched by a 3 M HCl solution at 80 °C for 3h and subsequently washed by deionized water to completely remove the nickel foam template. The obtained graphene foams (GFs) were dried under vacuum at 60 °C for 12 h. A typical area density of GF is ~ 0.15 mg cm^{-2}.

Atomic layer deposition (ALD) of ZnO on GF

The dry GF was placed into an atomic layer deposition system (MNT Micro &nanotech f-200) for ZnO deposition. High-purity nitrogen at 200 °C was used as a carrier gas for the whole process. To preserve the high conductivity of GF as much as possible, only 20 cycles of ALD were performed. Each cycle includes alternating flows of water (20 ms, oxidant) and diethyl zinc (20 ms, 99.999 %, Zn precursor) separated by flows of pure nitrogen gas (20 s and 20 s, respectively, carrier and cleaning gas). The thickness of deposited ZnO flakes on GF surfaces was estimated to be 3.7 nm according to a control sample of 150 cycles, 27.28 ± 0.035 nm thickness deposited on a silicon wafer, measured by ellipsometry (Table S1, Fig. S1). The as-obtained material was denoted as GF@ZnO.

Electrode preparation

A S-C electrode was fabricated by mixing 60 wt% sulfur with 30 wt% conductive carbon black (super-P) as a conducting agent and 10 wt% poly(vinylidene fluoride) (PVDF) as a binder in the N-methyl-2-pyrrolidone (NMP). The slurry was magnetic stirred for 24 h to achieve greater homogeneity. After stirring, the slurry was coated on an aluminum foil current collector with the thickness of 20 μm by a rolling machine, followed by a vacuum desiccation at 60 °C for 12 h. The coated electrodes were cut

into discs of diameter 13 mm. A typical mass loading of the active materials was ~ 1.5 mg cm^{-2}.

Materials characterization

The morphologies and elemental mapping of the GF and GF/GF@ZnO interlayers were observed using a scanning electron microscope (SEM, JEOL JSM-6510) and an energy dispersive X-ray spectrometer (EDS, PENTA FET Precision). The defect density and layer number of GF and GF@ZnO were estimated by Raman spectroscopy (Jobin YvonXploRA, HORIBA Scientific), excited by 532 nm laser. The ZnO atomic layer coating was characterized by using X-ray photoelectron spectroscopy (XPS, ESCALAB 250Xi, Thermo scientific) with Al Kα X-ray source.

Electrochemical measurements

The S-C electrode and interlayer were tested in two-electrode 2032 coin-type cells using Li foil as counter electrodes. The cells were assembled in an argon-filled glove box. The electrolyte was 1.0 M lithium bis(trifluoromethanesulfonyl)imide (LiTFSI) in dioxolane (DOL) and dimethoxyethane (DME) (1:1 by volume) with a 1.0 wt% (0.18 M) $LiNO_3$ additive (H_2O < 5 ppm). The GF (or GF@ZnO, or GF/GF@ZnO) interlayers were placed between the Celgard 2400 separator and S-C electrode working electrode, with the GF@ZnO side (when GF/GF@ZnO was applied) facing towards the lithium

counter electrode. Cyclic voltammetry (CV) was conducted at a scan rate of 0.1 mV s^{-1} in a voltage range of 1.5-3.0 V using Autolab PGSTAT302N electrochemical workstation. The electrochemical impedance spectroscopy (EIS) measurements were also carried out on the same workstation with an amplitude of 5 mV and a frequency range of 0.01Hz~100 kHz. Galvanostatic charge/discharge tests were performed in the potential range of 1.5-3.0 V at 25 °C with the Neware CT-4008 battery-testing system.

3. Results and discussion

Scheme 1 shows the configuration of the cell with GF-based interlayer. The interlayer is placed between a commercial separator and the S-C cathode, and the insert shows an image of the free-standing nature of as-prepared GF interlayer. To further enhance the polysulfides-blocking ability of the interlayer, we fabricated the ZnO modified GF (GF@ZnO) *via* ALD and overlapped it with pristine GF, which was denoted as GF/GF@ZnO. Different interlayers for example GF, 2GF (double-layered GF), GF@ZnO and GF/GF@ZnO were tested to show their effects on the electrochemical performance of S-C cathode. Specifically, the GF/GF@ZnO interlayer was inserted with the GF side towards cathode.

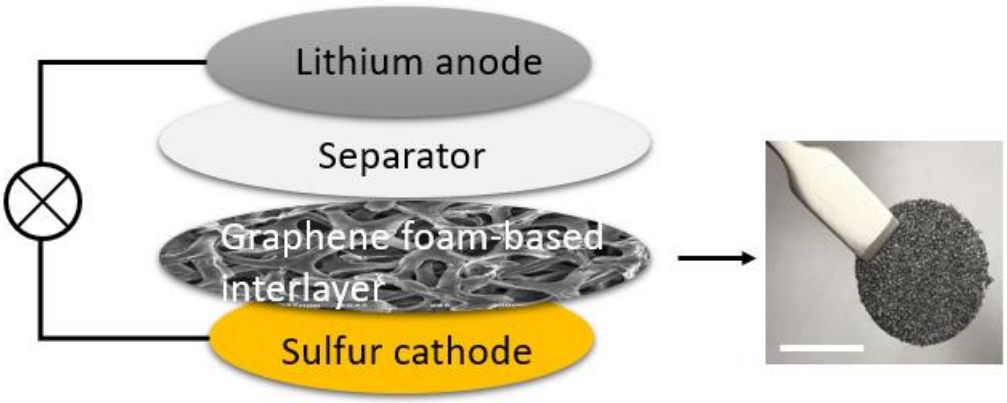

Scheme 1. A Li-S battery incorporated with a GF-based interlayer, with an insert showing a free-standing GF interlayer. The scale bar is 10 mm.

The structure and morphology characterizations of GF and GF@ZnO are shown in Fig. 1. The as-prepared GF and GF@ZnO show two prominent peaks at 1580 and 2718 cm^{-1} in Raman spectra (Fig.1a), corresponding to the G band and 2D band, respectively [56-58]. The low intensity band at 2445 cm^{-1} is the G* band [59]. Based on the integral intensity ratio of G band to 2D band (I_G/I_{2D} = 0.59) and the full width at half maximum (FWHM) of 2D, the graphene layers of GF are estimated to be 3~4 layers [59, 60] (see Table S2). In addition, the strongly suppressed defect-related D band (~1350 cm^{-1}) indicates overall high quality of the graphene in GF [55]. Due to the trace content of the ZnO, there was no obvious ZnO band in the Raman spectra (before 500 cm^{-1}), but the existence of ZnO is demonstrated by Zn 2p peak in XPS spectra (Fig. 1b), with an atomic percent of 0.79 % by XPS measurement. The GF perfectly inherits the interconnected 3D scaffold structure of the nickel foam template, and all the graphene sheets in the GF form hollow triangular prisms with a width of ~ 80 μm, as shown in

SEM images (Fig. 1c and the insert). The macroscale pores and interior hollow space encircled by few-layer GF sheets not only lead to rapid ionic transportation but also facilitate high electron conductivity, thus potentially reducing the polarization for the S-C electrode. To visualize the morphology of the deposited ZnO, the GF@ZnO was examined under high-resolution TEM (HRTEM), as shown in Fig. 1d. The deposited ZnO exhibits scattered nano-flakes morphology on the GF surface. This is likely resulting from the hydrophobic feature of the graphene surface in which no continuous nucleation sites are available to form ZnO. The HRTEM image of GF@ZnO (Fig.1e) is denoted with clear crystal lattice fringes with d-spacing of the (002) plane of the ZnO. The insert shows the layer structure of graphene edge with the fringe separation of 0.36 nm, in a good agreement with previous reported graphene structure [58].

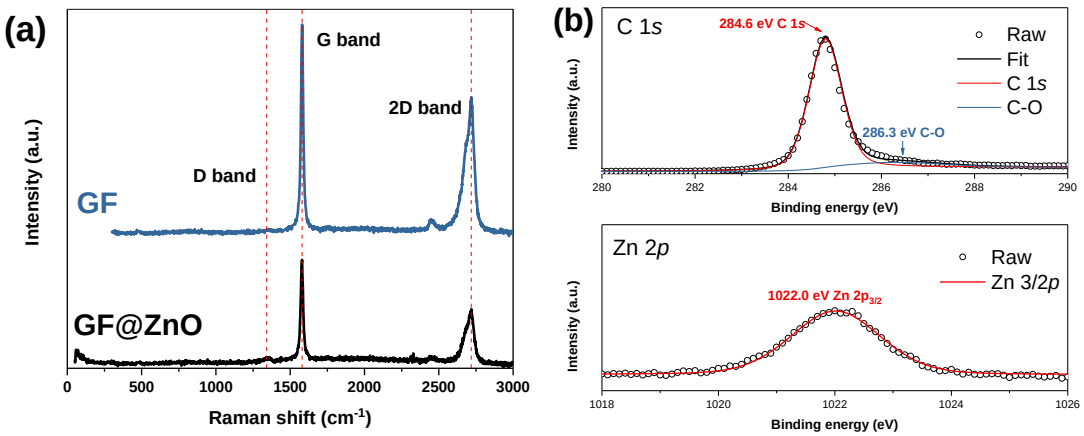

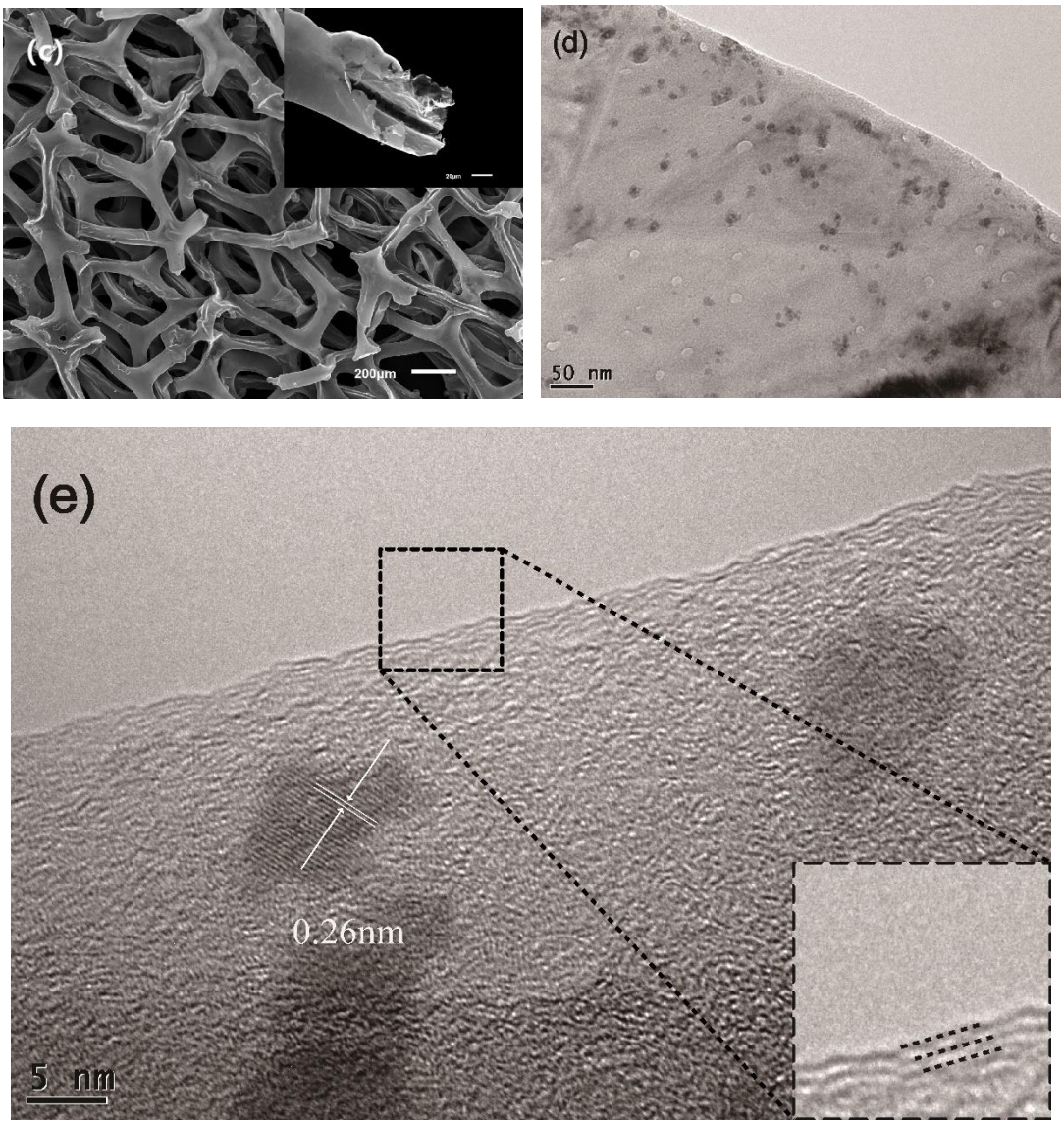

Fig. 1. (a) The Raman spectra of GF and GF@ZnO. (b) High resolution C 1*s* and Zn 2*p* XPS spectra of GF@ZnO. (c) SEM image of GF. The insert shows the fractured graphene triangular prism and its hollow interior space. (d) TEM image of the as-prepared GF@ZnO. (e) The HRTEM of GF@ZnO denoted with crystal lattice fringes with d-spacing of the (002) plane of the ZnO. The insert shows the layer structure of graphene edge.

Fig. 2 shows the cyclic voltammetry of S-C cell and cells with GF-based interlayers of the initial five cycles within a cutoff voltage window of 1.5-3.0 V at a scan rate of 0.1 mV s^{-1}. A double-layer GF (2GF) interlayer is applied here for a more accurate

comparative evaluation with GF/GF@ZnO double-layer interlayer. During the initial cycle, the cell without interlayer exhibits two broad cathodic peaks at around 1.75 and 1.85 V, which are related to the redox state from elemental sulfur to high-order polysulfides and further reduction to Li_2S_2/Li_2S, respectively [46]. The one broad anodic peak at around 2.58 V corresponds to the conversion of Li_2S_2/Li_2S to high-order polysulfides and elemental sulfur [37]. The shifts in the anodic peaks between the initial and following cycles are possibly due to the migration of the active sulfur to more electrochemically stable sites [22, 33, 46]. During the following cycles, the anodic peaks gradually shift to a lower potential, indicating the instability of pristine S-C electrode during cycling. Meanwhile, the CV curves of cell with 2GF interlayer show similar shapes, but the anodic peak width becomes much narrower (shrinking from 0.61 V to 0.35 V) and higher than that of S-C cell (from ~1.1 A g^{-1} to ~1.5 A g^{-1}), indicating that the redox reaction takes place easier in cell with 2GF interlayer. The cathodic peaks shift to higher potentials at 1.99 and 2.29 V respectively, and display narrower peak widths compared to those of S-C cells, suggesting the cell with 2GF interlayer has less polarization and higher conductivity than the pristine S-C cell. Except for the initial cycle, the CV curves of the cell with 2GF interlayer overlap without obvious shift in peak location, demonstrating the good cycling stability and reaction reversibility of this Li-S cell. The cells with GF@ZnO and GF/GF@ZnO interlayers (Figs. 2c and 2d) exhibit similar CV profiles in Fig. 2b, but possess more intense anodic peaks (1.6-2.0 A g^{-1})). Meanwhile the redox peaks in these two cells reveal less shifting from the second cycling. These variations can be ascribed to the higher sulfur utilization

efficiency brought by the ZnO layer.

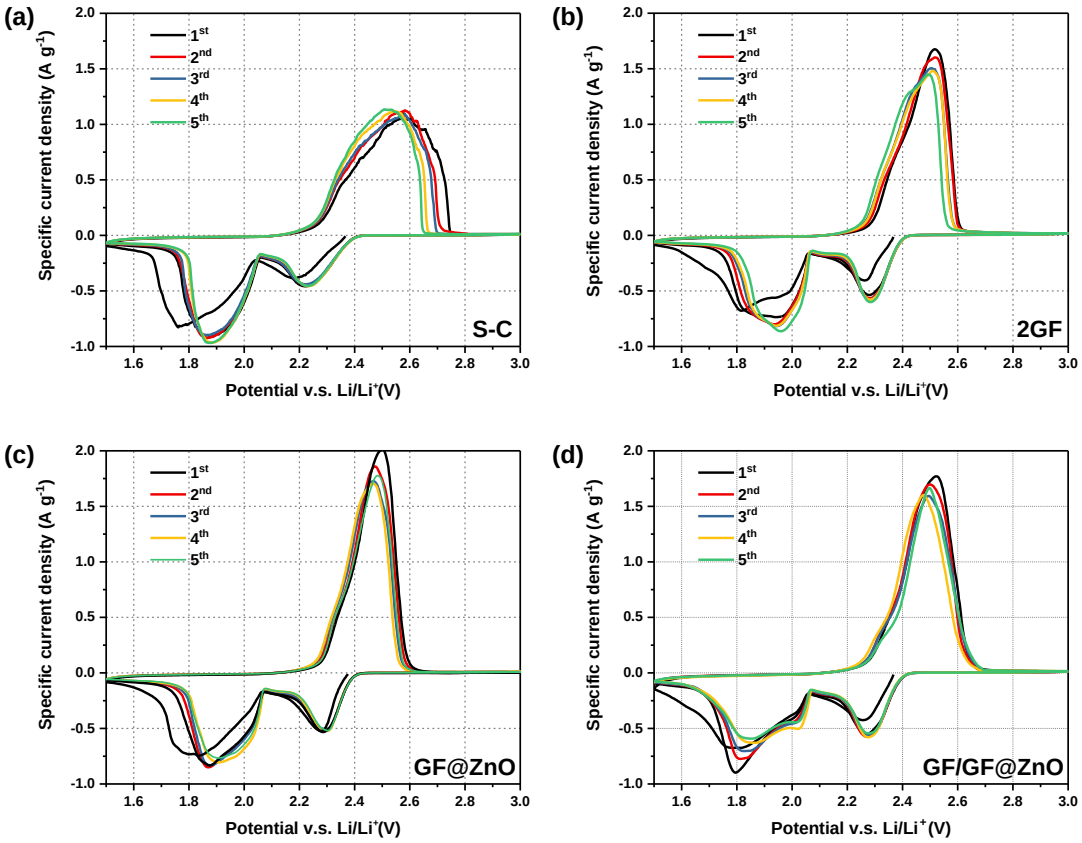

Fig. 2. Cyclic voltammetry profiles of the initial five cycles of the S-C cell and cells with 2GF, GF@ZnO and GF/GF@ZnO interlayers, respectively.

The initial galvanostatic charge/discharge behaviors of different Li–S batteries evaluated at a current density of 0.5 C are shown in Fig. 3a. Two discharge plateaus and one charge plateau can be observed for all the cells, which are consistent with the CV plots. For pristine S-C cathode cell, it delivers an initial specific capacity of 595 mAh g^{-1}), corresponding 35.5 % of the theoretical capacity (1675 mAh g^{-1}). On the other hand, cells with different interlayers exhibit higher specific capacity and longer

charge/discharge plateaus, indicating that the GF-based interlayers can effectively improve the sulfur utilization. The meliorated specific capacity surges to 735, 805, and 1051 mAh g^{-1} with the application of 2GF, GF@ZnO and GF/GF@ZnO interlayers, respectively. In particular, the cell with GF/GF@ZnO interlayer has the longest plateaus, with the lowest voltage hysteresis (ΔE_4) of 233 mV (vs ΔE_1 =326 mV for S-C, ΔE_2 =237 mV for 2GF and ΔE_3 =235mV for GF@ZnO) at 0.5 C, which suggests a more kinetically favored electrochemical redox reaction process and low internal resistance in the cell with GF/GF@ZnO interlayer [61, 62]. In addition, the capacities for high voltage plateau and low voltage plateau follow the order of $C_1>C_2>C_3>C_4$, confirming the same order of the abilities for sulfur utilization when using different interlayers in the cells.

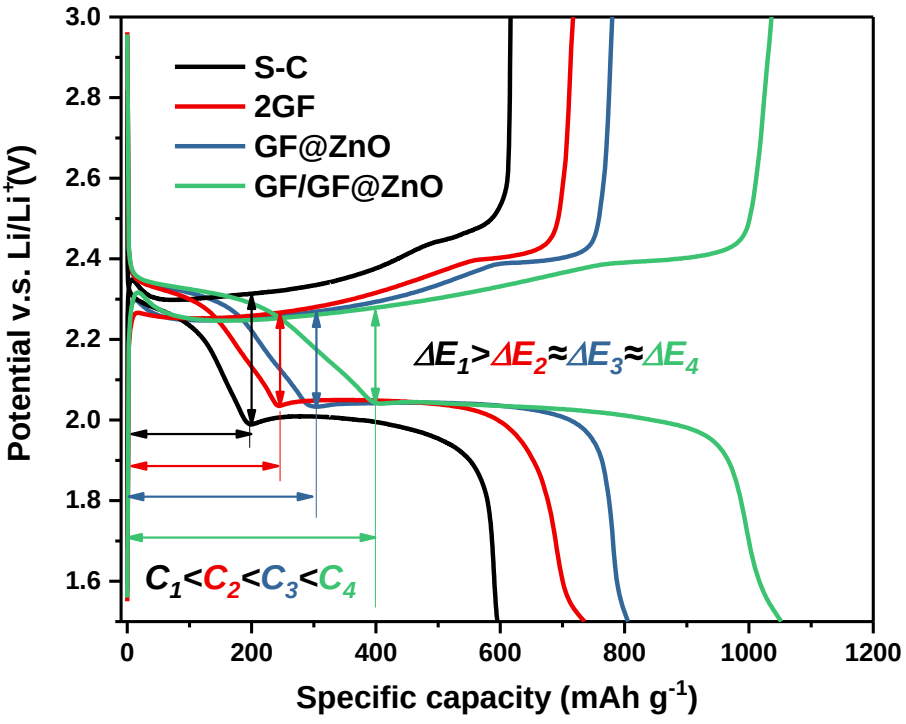

Fig. 3. The initial galvanostatic charge-discharge profiles of S-C cell and cells with 2GF, GF@ZnO and GF/GF@ZnO interlayers at 0.5 C.

Fig.4a presents the cyclic performance of the cells with different interlayers measured at a galvanostatic charge/discharge current of 0.5 C and 0.5 C between 1.5 and 3 V. At current density of 0.5 C, the cell with pristine S-C cathode exhibits a low initial specific capacity of 681 mAh g^{-1}, taking up only 40.6 % of the theoretical value. After 100 cycles, it drops to 326 mAh g^{-1}, with a capacity degradation of 0.52 % per cycle. In contrast, the cells with 2GF and GF@ZnO interlayers show higher initial capacities of 735 and 805 mAh g^{-1}, retaining a capacity of 386 and 595 mAh g^{-1} after 100 cycles, with a relatively lower capacity decay of 0.47 % and 0.26 % per cycle. A control experiment showed that different ALD cycles (20, 60 and 80 cycles) do not influence the capacity performance remarkably (Fig. S2), so a minimum cycle (20) was selected for all the following experiments in this study. The GF/GF@ZnO interlayer delivers an improved initial capacity of 1051 mAh g^{-1} and a stable residual capacity of 672 mAh g^{-1} after 100 cycles, with a capacity decay of 0.36 % per cycle. The enhanced initial and residual specific capacity of the GF/GF@ZnO interlayer modified Li-S battery can be ascribed to the doubled area density of GF interlayer, which reduces the chance of polysulfides escaping through the macro-pores in GF interlayer. Another contribution to enhance the specific capacity is probably related to the chemically trapping the polysulfides by the ZnO coating. The interlayer with reverse orientation (namely the GF@ZnO side towards the cathode) was also tested, the GF@ZnO/GF

shows cycling capacity very close to that of GF/GF@ZnO, with slightly lower Coulombic efficiency during the first 50 cycles (as shown in Fig. S3). The negligible difference between these two kinds of cells reveals that the hundred micron-scale porosity of the GF provides sufficient space for the out-layer GF to get contact with the cathode surface, therefore both layers are functioning in either situations. For the consistency of data, only the cell of GF/GF@ZnO will be discussed in the following section. We also tested the triple-layer GF/GF/GF@ZnO interlayer to check the effect of increasing the interlayer thickness onthe improvement of the capacity performance. However, compared with the GF/GF@ZnO cell, it seems that the additional GF layer decreases the specific capacity performance of the sulfur cathode. Not only the initial capacity drops from ~1050 to ~700 mAh g^{-1}, the capacity after 50 cycles of the GF/GF/GF@ZnO is also 100 mAh g^{-1} less than the GF/GF@ZnO one. Hence, the bi-layer GF/GF@ZnO is proved to be the optimum interlayer structure. Although the additional GF might provide more polysulfide-trapping sites, it hinders the transmission of Li ion from anode side to cathode, and this drawback cannot be compensated by the advantage from thickness increase, which synthetically results in capacity shrinkage. To emphasize the negligible mass addition of the interlayer, the cycling specific capacity performance based on the mass of cathode materials (including super-P, binder and interlayer) is shown in Fig. 4b, in which the cells with GF@ZnO and GF/GF@ZnO interlayers still show enhanced specific capacities. This proves the lightness of the GF-based interlayers can effectively improve the cell without impairing the overall specific capacity.

The high rate capabilities of the cells with different interlayers are shown in Fig. 4c. It is clearly seen that with the gradually growing of current rate, the specific capacity of the cells with GF-based interlayers is much higher than that of cell without interlayer at the same rate. Among all cells, the cell with GF/GF@ZnO interlayer presents the highest initial discharge capacity of 1013 mAh g^{-1} at 0.2 C. When the current rate gradually increases from 0.2 to 0.5, 1 and 2 C after every 10 cycles, the cell with GF/GF@ZnO delivers high and stable discharge capacities of 914, 721, 613 and 518 mAh g^{-1}, respectively. After the rate reverts to 0.5 C, the capacity recovers to 688 mAh g^{-1}, demonstrating excellent stability and reversibility of the Li-S cell with the GF/GF@ZnO interlayer.

To further evaluate the improvement of different GF-based interlayers on electrochemical performance, the electrochemical impedance spectroscopy measurements were conducted on fresh cell of S-C cathode and cells with different GF-based interlayers, and the corresponding Nyquist plots and equivalent circuits are shown in Fig.4d and 4e. In the Nyquist plots, the diameter of the depressed semicircle in the high-to-medium frequency region corresponds to charge-transfer resistance (R_{ct}), while the sloping line in the low-frequency region is assigned to Warburg impedance (W_o), which reflects the diffusion process of the polysulfides [33, 41, 63, 64]. The sum of R_e, R_{ct} and R_{st} is calculated as the total resistance of the cell (R_{total}) [40]. According to the fitted results (Table 1), the most prominent difference between these two cells is the shrinkage in R_{ct} values after interlayers inserting. This amelioration should be

ascribed to the highly conductive few-layer graphene foam that acts as the secondary current collector, which greatly facilitates the redox of dissolved polysulfides. The low R_{ct} values of cells with interlayers indicate the highest efficiency interlayers in reutilizing polysulfides. It is noticeable that an additional semicircle in high-frequency region appeals in the Nyquist plot of the cell with interlayers, which corresponds to the interface resistance (R_{st}) [44, 61]. This is probably caused by the additional thickness brought by the interlayer [41, 65]. The low R_{total} value of the cell with GF/GF@ZnO interlayer is another evidence of the remarkable effect of this double-layer interlayer on reducing the internal resistance.

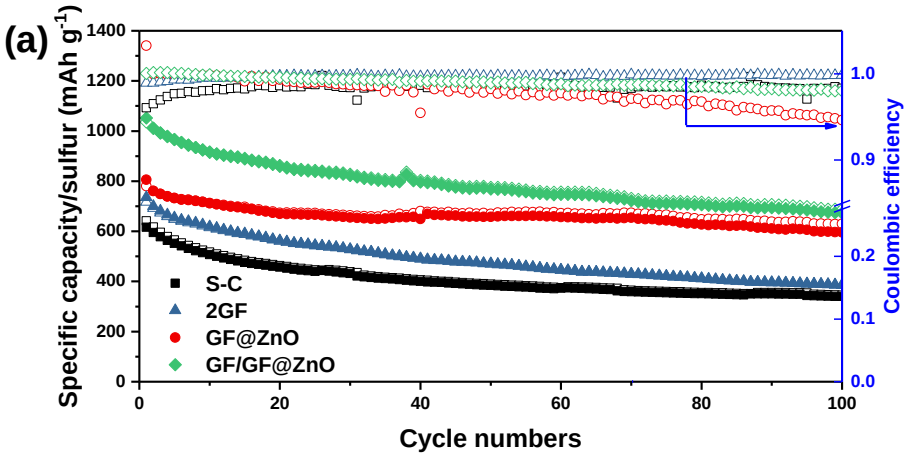

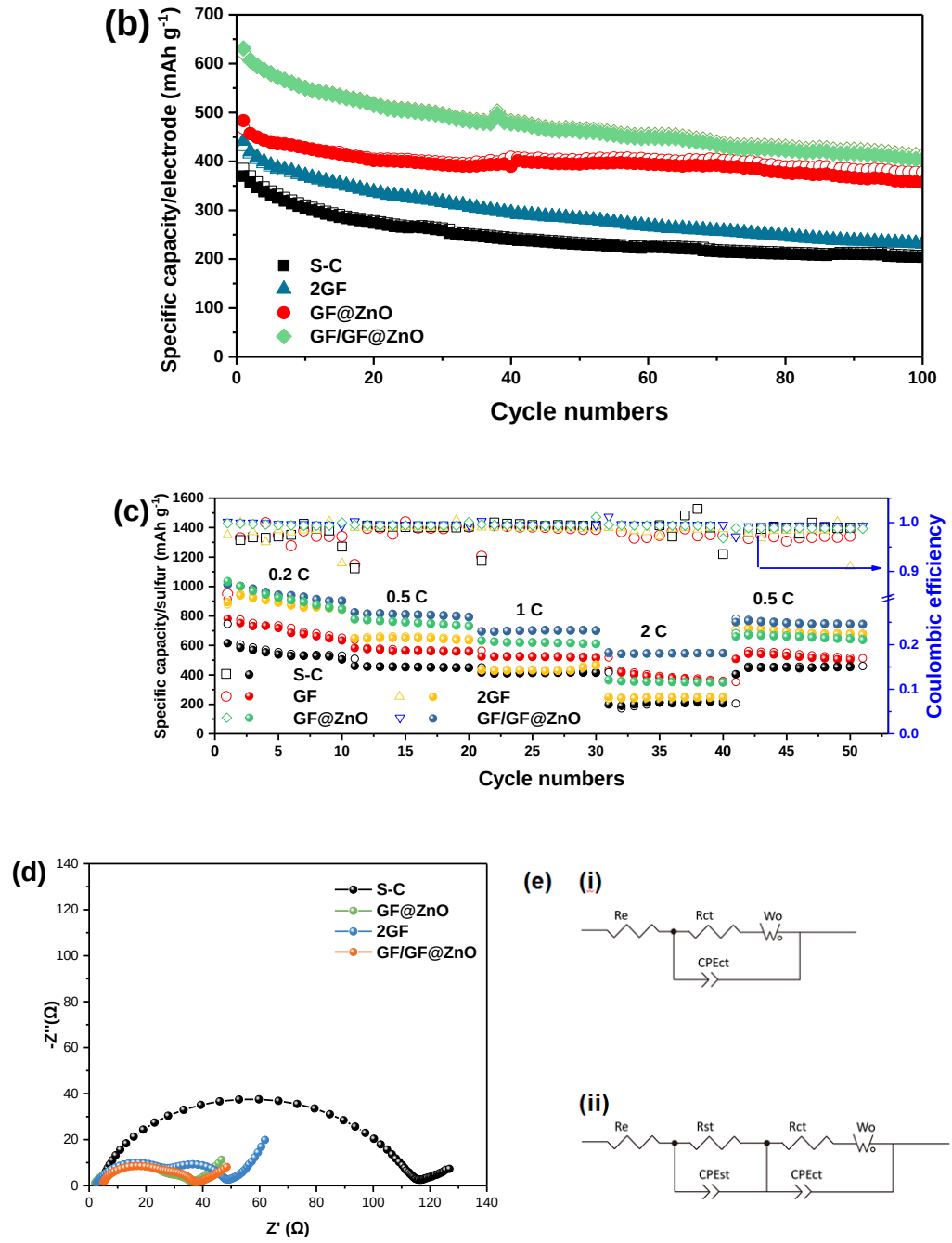

Fig.4. Electrochemical performance of Li-S cells with different interlayers: (a) cyclic test performance of cells with different interlayers measured at 0.5 C and (b) the corresponding cycling specific capacity based on cathode and interlayer mass. (c) Rate performance and (d) electrochemical impedance spectra of cells with different interlayers before cycling; and (e) the corresponding equivalent circuit: (i) pristine Li-S battery and (ii) cells with different interlayers.

Table 1. The fitting results of R_e, R_{ct}, R_{st} and R_{total} values of cells with 2GF, GF@ZnO

and GF/GF@ZnO interlayer and without interlayer.

	R_e (Ω)	R_{ct} (Ω)	R_{st} (Ω)	R_{total} (Ω)
Cell without interlayer	3.9	110	-	113.9
Cell with GF/GF@ZnO interlayer	4.3	14.0	20.2	38.5
Cell with 2GF interlayer	2.2	27.9	17.2	47.3
Cell with GF@ZnO interlayer	1.5	6.1	28.4	36.0

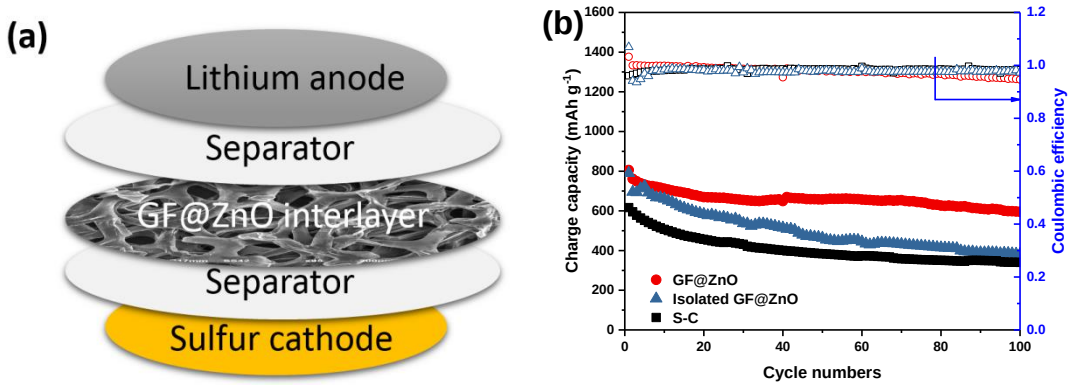

Fig.5. (a) Scheme of the cell with an isolated interlayer. (b) The cyclic discharge specific capacity performance of the cell with GF@ZnO interlayer, isolated GF@ZnO interlayer and pristine cathode at 0.5 C.

To highlight the importance of the interlayer in trapping the polysulfides, a control experiment was conducted where the GF@ZnO interlayer was placed in the cell but electronically isolated, as shown in Fig. 5(a). An extra separator was used to avoid the contact between sulfur cathode and interlayer. Compared with the cell with the GF@ZnO interlayer, the cell with isolated separator shows impaired specific capacity.

After 100 cycles at 0.5 C, it drops to 382 mAh g^{-1}, which is much lower than the 595 mAh g^{-1} of the GF@ZnO cell and is close to that of the pristine Li-S cell (340 mAh g^{-1}). Due to the extra separation between sulfur cathode and interlayer, the GF@ZnO is electronically isolated and the trapped polysulfides on the interlayer cannot be utilized during the following cycles, resulting in fast capacity degrading. During the initial 50 cycles, the cell with isolated interlayer exhibited higher capacity than pristine cell, which could be attributed to the suppressed passivation layer on the Li anode surface [66].

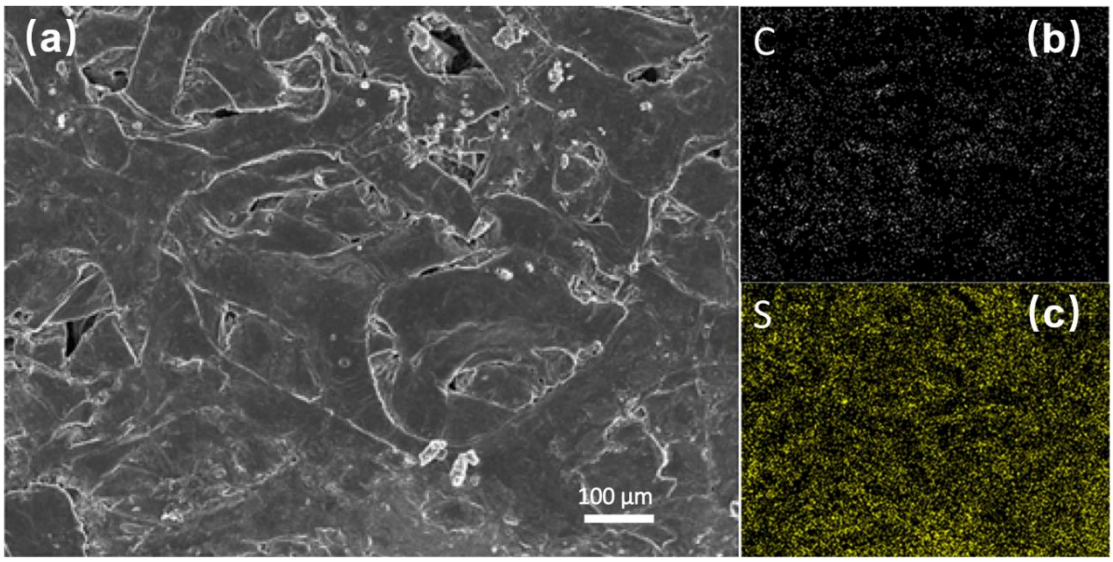

Fig.6. (a) SEM image of the GF/GF@ZnO interlayer after 100 cycles at 0.5 C; (b) corresponding EDS carbon elemental mapping and (c) corresponding EDS sulfur elemental mapping.

The SEM image and the elemental mapping of C and S for the GF/GF@ZnO interlayer surface towards the cathode confirm the entrapment of active material. After

100 cycles at 0.5 C, the GF/GF@ZnO interlayer is taken out from the disassembled cell and characterized by SEM and EDS mapping, as shown in Fig. 6. The SEM image reveals an intact structure of this GF-based interlayer with no prominent damage, suggesting its high mechanical tolerance for volumetric variation of sulfur cathode during cycling. In addition, the elemental mapping shows that carbon and sulfur signals distribute evenly on the side towards cathode without any evident agglomeration of active sulfur. The Ni foam-templated GF shows hierarchical porosity with a rather high proportion of micropores agreed well with a literature [67], which is valuable in reserving polysulfides. This mapping result confirms the function of GF/GF@ZnO interlayer as a co-current collector and recycler of the dissolved polysulfides species. Meanwhile, EDS mapping of the GF@ZnO side towards the separator was also conducted and it shows similar morphology with the GF side (Fig. S5.). However, it has stronger sulfur signal than that of GF side, proving the polysulfides trapping ability brought by the ZnO. A comparison of EDS quantitative measurement between the cycled single-layer GF and GF@ZnO also confirms the role of ZnO as the polysulfide trapper (Fig. S6).

To identify the standing of this work among published results, a comparison (as shown in Table 2) is made of electrochemical performance between the current work and the cells with carbon-based and other interlayers. A parameter called "cycled capacity increment efficiency ($A \cdot h \cdot cm^2\ g^{-2}$)" is introduced here to evaluate the interlayers' ability to improve capacity performance by density after cycling. The

cycled capacity increment efficiency (Δc) is calculated as follows:

$$\Delta c = \frac{C_{interlayer} - C_{bare}}{\rho_{interlayer}}$$

Where $C_{interlayer}$ represents the specific capacity of cell with interlayer after certain cycles, and C_{bare} is the specific capacity of the same cell without interlayer after the same cycles. The parameter $\rho_{interlayer}$ is the density of interlayer, and here the areal density is adopted for the convenience of measurement. This Δc parameter is important to evaluate the comprehensive effect of interlayer on sulfur cathode, especially the degree of interlayer to "dilute" the capacity density of cathode. In this case, the effect of the additional mass of interlayer on the capacity density of cathode should be also considered. The higher the Δc is, the more effective an interlayer can be. Compared with all the other interlayers for Li-S batteries, the optimal GF/GF@ZnO interlayer shows a higher Δc value (1090 $Ahcm^2\ g^{-2}$) than most other interlayers, such as Fe_3C/carbon nanofiber [42], MnO_2@graphene [68], activated carbon nanofiber [10], and super-P [69]. Although the Nafion/super-P [41] shows a higher Δc value, the GF/GF@ZnO presents a much higher initial discharge capacity and residual capacity after cycles at the same current rate, compensating the overall capacity performance.

Table 2. Comparison of electrochemical performance of Li-S batteries with different interlayers and corresponding Δc parameters.

Interlayer	Current rate	Cycle	Initial	Residual	Interlayer	Cycled capacity	Ref.

materials	($mA\ g^{-1}$)	numbers	discharge capacity ($mAh\ g^{-1}$)	reversible capacity ($mAh\ g^{-1}$)	areal density ($mg\ cm^{-2}$)	increment efficiency Δc ($Ahcm^2\ g^{-2}$)	
Activated carboncloth @Al_2O_3	220	40	~1150	766	7.89	69.1	[16]
Fe_3C/carbon nanofiber	200	100	1177	893	2.26	218.1	[42]
Nafion/super-P	837	250	863	430	0.15	1666.6	[41]
Polypyrrole nanotube film	335	200	~1340	890	1.0	603	[70]
Polypyrrole	335	100	719	~850	0.3	833.3	[43]
MnO_2@graphene	837	100	1395	600	0.8	625	[68]
Activated carbon nanofiber	Not given	100	~1200	897	1.0	851	[10]
Super-P	167.5	50	~990	~800	1.0-1.5	200-266.7	[69]
GF/GF@ZnO	837	100	1051	672	0.3	1090	This work

4. Conclusion

In this work, the light-weight and free-standing GF-based interlayers are synthesized by a facile CVD process and modified by a thin layer of ZnO using ALD method. Being used as the interlayers between sulfur cathode and the separator, the GF-based interlayers prove their effectiveness in serving as an electron high-way and entrapping the dissolved polysulfides. The GF/GF@ZnO interlayer shows the best amelioration for Li-S batteries, with an initial specific capacity of 1051 mAh g^{-1} and a revertible capacity of 672 mAh g^{-1} at 0.5 C for 100 cycles. Remarkably, the mass addition of this interlayer on the total cathode is less than 5 wt. %. This work highlights that the GF-based interlayers are suitable to improve capacity and cycling performance of Li-S batteries without undermining their overall energy density.

Acknowledgments

This work was supported by the National Natural Science Foundation of China (NSFC Grants 21750110441), Suzhou Science and Technology programme (SYG 201623), Suzhou Industrial Park Initiative Platform Development for Suzhou Municipal Key Lab for New Energy Technology (RR0140), and Key Program Special Fund in XJTLU (KSF-A-04).

Reference

[1] Stankovich, S., R.D. Piner, X. Chen, N. Wu, S.T. Nguyen, and R.S. Ruoff, *Stable aqueous dispersions of graphitic nanoplatelets via the reduction of exfoliated graphite oxide in the presence of poly(sodium 4-styrenesulfonate).* J. Mater. Chem., 2006. **16**(2): p. 155-158.

[2] Wu, F., J.T. Lee, A. Magasinski, H. Kim, and G. Yushin, *Solution-Based Processing of Graphene-Li2S Composite Cathodes for Lithium-Ion and Lithium-Sulfur Batteries.* Particle & Particle Systems Characterization, 2014. **31**(6): p. 639-644.

[3] Manthiram, A., S.H. Chung, and C. Zu, *Lithium-sulfur batteries: progress and prospects.* Adv Mater, 2015. **27**(12): p. 1980-2006.

[4] Xu, J., J. Ma, Q. Fan, S. Guo, and S. Dou, *Recent Progress in the Design of Advanced Cathode Materials and Battery Models for High-Performance Lithium-X (X = O_2 , S, Se, Te, I_2 , Br_2) Batteries.* Adv Mater, 2017. **29**(28): p. 1606454.

[5] Zhang, L., L. Ji, P.A. Glans, Y. Zhang, J. Zhu, and J. Guo, *Electronic structure and chemical bonding of a graphene oxide-sulfur nanocomposite for use in superior performance lithium-sulfur cells.* Phys Chem Chem Phys, 2012. **14**(39): p. 13670-5.

[6] Dong, K., S. Wang, H. Zhang, and J. Wu, *Preparation and electrochemical performance of sulfur-alumina cathode material for lithium-sulfur batteries.* Materials Research Bulletin, 2013. **48**(6): p. 2079-2083.

[7] Zheng, C., S. Niu, W. Lv, G. Zhou, J. Li, S. Fan, Y. Deng, Z. Pan, B. Li, F. Kang, and Q.-H. Yang, *Propelling polysulfides transformation for high-rate and long-life lithium–sulfur batteries.* Nano Energy, 2017. **33**: p. 306-312.

[8] Sun, F., J. Wang, D. Long, W. Qiao, L. Ling, C. Lv, and R. Cai, *A high-rate lithium–sulfur battery assisted by nitrogen-enriched mesoporous carbons decorated with ultrafine La2O3 nanoparticles.* Journal of Materials Chemistry A, 2013. **1**(42): p. 13283.

[9] Kim, T.-H., J.-S. Park, S.K. Chang, S. Choi, J.H. Ryu, and H.-K. Song, *The Current Move of Lithium Ion Batteries Towards the Next Phase.* Advanced Energy Materials, 2012. **2**(7): p. 860-872.

[10] Wang, J., Y. Yang, and F. Kang, *Porous carbon nanofiber paper as an effective interlayer for high-performance lithium-sulfur batteries.* Electrochimica Acta, 2015. **168**: p. 271-276.

[11] Scrosati, B., J. Hassoun, and Y.-K. Sun, *Lithium-ion batteries. A look into the future.* Energy & Environmental Science, 2011. **4**(9): p. 3287.

[12] Lei, T., W. Chen, J. Huang, C. Yan, H. Sun, C. Wang, W. Zhang, Y. Li, and J. Xiong, *Multi-Functional Layered WS_2 Nanosheets for Enhancing the Performance of Lithium-Sulfur*

Batteries. Advanced Energy Materials, 2017. **7**(4): p. 1601843.

[13] Zhao, Y., W. Zhu, G.Z. Chen, and E.J. Cairns, *Polypyrrole/TiO_2 nanotube arrays with coaxial heterogeneous structure as sulfur hosts for lithium sulfur batteries.* Journal of Power Sources, 2016. **327**: p. 447-456.

[14] Wei Seh, Z., W. Li, J.J. Cha, G. Zheng, Y. Yang, M.T. McDowell, P.C. Hsu, and Y. Cui, *Sulphur-TiO_2 yolk-shell nanoarchitecture with internal void space for long-cycle lithium-sulphur batteries.* Nat Commun, 2013. **4**: p. 1331.

[15] Zhu, J., C. Chen, Y. Lu, J. Zang, M. Jiang, D. Kim, and X. Zhang, *Highly porous polyacrylonitrile/graphene oxide membrane separator exhibiting excellent anti-self-discharge feature for high-performance lithium–sulfur batteries.* Carbon, 2016. **101**: p. 272-280.

[16] Han, X., Y. Xu, X. Chen, Y.-C. Chen, N. Weadock, J. Wan, H. Zhu, Y. Liu, H. Li, G. Rubloff, C. Wang, and L. Hu, *Reactivation of dissolved polysulfides in Li–S batteries based on atomic layer deposition of Al_2O_3 in nanoporous carbon cloth.* Nano Energy, 2013. **2**(6): p. 1197-1206.

[17] Liang, X., Y. Rangom, C.Y. Kwok, Q. Pang, and L.F. Nazar, *Interwoven MXene Nanosheet/Carbon-Nanotube Composites as Li-S Cathode Hosts.* Adv Mater, 2017. **29**(3): p. 1-7.

[18] Cao, K., H. Liu, Y. Li, Y. Wang, and L. Jiao, *Encapsulating sulfur in δ-MnO_2 at room temperature for Li-S battery cathode.* Energy Storage Materials, 2017. **9**: p. 78-84.

[19] Li, L., G. Zhou, L. Yin, N. Koratkar, F. Li, and H.-M. Cheng, *Stabilizing sulfur cathodes using nitrogen-doped graphene as a chemical immobilizer for Li S batteries.* Carbon, 2016. **108**: p. 120-126.

[20] Xiong, D., X. Li, Z. Bai, and S. Lu, *Recent Advances in Layered Ti_3C_2Tx MXene for Electrochemical Energy Storage.* Small, 2018. **14**(17): p. e1703419.

[21] Zhu, J., M. Yanilmaz, K. Fu, C. Chen, Y. Lu, Y. Ge, D. Kim, and X. Zhang, *Understanding glass fiber membrane used as a novel separator for lithium–sulfur batteries.* Journal of Membrane Science, 2016. **504**: p. 89-96.

[22] Zhu, J., Y. Ge, D. Kim, Y. Lu, C. Chen, M. Jiang, and X. Zhang, *A novel separator coated by carbon for achieving exceptional high performance lithium-sulfur batteries.* Nano Energy, 2016. **20**: p. 176-184.

[23] Han, S.-C., M.-S. Song, H. Lee, H.-S. Kim, H.-J. Ahn, and J.-Y. Lee, *Effect of Multiwalled Carbon Nanotubes on Electrochemical Properties of Lithium/Sulfur Rechargeable Batteries.* Journal of The Electrochemical Society, 2003. **150**(7): p. A889.

[24] Guo, J., Y. Xu, and C. Wang, *Sulfur-impregnated disordered carbon nanotubes cathode for lithium-sulfur batteries.* Nano Lett, 2011. **11**(10): p. 4288-94.

[25] Liu, Y., X. Zhao, G.S. Chauhan, and J.-H. Ahn, *Nanostructured nitrogen-doped mesoporous carbon derived from polyacrylonitrile for advanced lithium sulfur batteries.* Applied Surface Science, 2016. **380**: p. 151-158.

[26] Hao, Y., D. Xiong, W. Liu, L. Fan, D. Li, and X. Li, *Controllably Designed "Vice-Electrode" Interlayers Harvesting High Performance Lithium Sulfur Batteries.* ACS Appl Mater Interfaces, 2017. **9**(46): p. 40273-40280.

[27] Wu, F., J. Chen, L. Li, T. Zhao, and R. Chen, *Improvement of Rate and Cycle Performence by Rapid Polyaniline Coating of a MWCNT/Sulfur Cathode.* The Journal of Physical Chemistry C, 2011. **115**(49): p. 24411-24417.

[28] Xiao, L., Y. Cao, J. Xiao, B. Schwenzer, M.H. Engelhard, L.V. Saraf, Z. Nie, G.J. Exarhos, and J. Liu, *A soft approach to encapsulate sulfur: polyaniline nanotubes for lithium-sulfur batteries with long cycle life.* Adv Mater, 2012. **24**(9): p. 1176-81.

[29] Chen, H., W. Dong, J. Ge, C. Wang, X. Wu, W. Lu, and L. Chen, *Ultrafine sulfur nanoparticles in conducting polymer shell as cathode materials for high performance lithium/sulfur batteries.* Sci Rep, 2013. **3**: p. 1910.

[30] Liang, X. and L.F. Nazar, *In Situ Reactive Assembly of Scalable Core-Shell Sulfur-MnO_2 Composite Cathodes.* ACS Nano, 2016. **10**(4): p. 4192-8.

[31] Hu, N., X. Lv, Y. Dai, L. Fan, D. Xiong, and X. Li, *SnO_2/Reduced Graphene Oxide Interlayer Mitigating the Shuttle Effect of Li-S Batteries.* ACS Appl Mater Interfaces, 2018. **10**(22): p. 18665-18674.

[32] Xing, L.-B., K. Xi, Q. Li, Z. Su, C. Lai, X. Zhao, and R.V. Kumar, *Nitrogen, sulfur-codoped graphene sponge as electroactive carbon interlayer for high-energy and -power lithium–sulfur batteries.* Journal of Power Sources, 2016. **303**: p. 22-28.

[33] Wang, Z., J. Zhang, Y. Yang, X. Yue, X. Hao, W. Sun, D. Rooney, and K. Sun, *Flexible carbon nanofiber/polyvinylidene fluoride composite membranes as interlayers in high-performance LithiumSulfur batteries.* Journal of Power Sources, 2016. **329**: p. 305-313.

[34] Zhang, Z., G. Wang, Y. Lai, and J. Li, *A freestanding hollow carbon nanofiber/reduced graphene oxide interlayer for high-performance lithium–sulfur batteries.* Journal of Alloys and Compounds, 2016. **663**: p. 501-506.

[35] Su, Y.S. and A. Manthiram, *Lithium-sulphur batteries with a microporous carbon paper as a bifunctional interlayer.* Nat Commun, 2012. **3**: p. 1166.

[36] Su, Y.S. and A. Manthiram, *A new approach to improve cycle performance of rechargeable lithium-sulfur batteries by inserting a free-standing MWCNT interlayer.* Chem Commun (Camb), 2012. **48**(70): p. 8817-9.

[37] Zhang, K., F. Qin, J. Fang, Q. Li, M. Jia, Y. Lai, Z. Zhang, and J. Li, *Nickel foam as interlayer to improve the performance of lithium–sulfur battery.* Journal of Solid State Electrochemistry, 2013. **18**(4): p. 1025-1029.

[38] Zhang, K., Q. Li, L. Zhang, J. Fang, J. Li, F. Qin, Z. Zhang, and Y. Lai, *From filter paper to carbon paper and toward Li–S battery interlayer.* Materials Letters, 2014. **121**: p. 198-201.

[39] Chung, S.H. and A. Manthiram, *A hierarchical carbonized paper with controllable thickness as a modulable interlayer system for high performance Li-S batteries.* Chem Commun (Camb), 2014. **50**(32): p. 4184-7.

[40] Wang, Q., Z. Wen, J. Yang, J. Jin, X. Huang, X. Wu, and J. Han, *Electronic and ionic co-conductive coating on the separator towards high-performance lithium–sulfur batteries.* Journal of Power Sources, 2016. **306**: p. 347-353.

[41] Hao, Z., L. Yuan, Z. Li, J. Liu, J. Xiang, C. Wu, R. Zeng, and Y. Huang, *High performance lithium-sulfur batteries with a facile and effective dual functional separator.* Electrochimica Acta, 2016. **200**: p. 197-203.

[42] Huang, J.-Q., B. Zhang, Z.-L. Xu, S. Abouali, M. Akbari Garakani, J. Huang, and J.-K. Kim, *Novel interlayer made from Fe3C/carbon nanofiber webs for high performance lithium–sulfur batteries.* Journal of Power Sources, 2015. **285**: p. 43-50.

[43] Ma, G., Z. Wen, J. Jin, M. Wu, X. Wu, and J. Zhang, *Enhanced cycle performance of Li–S battery with a polypyrrole functional interlayer.* Journal of Power Sources, 2014. **267**: p. 542-546.

[44] Huang, J.-Q., Z.-L. Xu, S. Abouali, M. Akbari Garakani, and J.-K. Kim, *Porous graphene oxide/carbon nanotube hybrid films as interlayer for lithium-sulfur batteries.* Carbon, 2016. **99**: p. 624-632.

[45] Zhao, T., Y. Ye, X. Peng, G. Divitini, H.-K. Kim, C.-Y. Lao, P.R. Coxon, K. Xi, Y. Liu, C. Ducati, R. Chen, and R.V. Kumar, *Advanced Lithium-Sulfur Batteries Enabled by a Bio-Inspired Polysulfide Adsorptive Brush.* Advanced Functional Materials, 2016. **26**(46): p. 8418-8426.

[46] Xiao, Z., Z. Yang, L. Wang, H. Nie, M. Zhong, Q. Lai, X. Xu, L. Zhang, and S. Huang, *A Lightweight TiO_2/Graphene Interlayer, Applied as a Highly Effective Polysulfide Absorbent for Fast, Long-Life Lithium-Sulfur Batteries.* Adv Mater, 2015. **27**(18): p. 2891-8.

[47] Tao, X., J. Wang, C. Liu, H. Wang, H. Yao, G. Zheng, Z.W. Seh, Q. Cai, W. Li, G. Zhou, C. Zu, and Y. Cui, *Balancing surface adsorption and diffusion of lithium-polysulfides on nonconductive oxides for lithium-sulfur battery design.* Nat Commun, 2016. **7**: p. 11203.

[48] Liang, X., C. Hart, Q. Pang, A. Garsuch, T. Weiss, and L.F. Nazar, *A highly efficient polysulfide mediator for lithium-sulfur batteries.* Nat Commun, 2015. **6**: p. 5682.

[49] Gu, X., C.-j. Tong, B. Wen, L.-m. Liu, C. Lai, and S. Zhang, *Ball-milling synthesis of ZnO@sulphur/carbon nanotubes and Ni(OH)2@sulphur/carbon nanotubes composites for high-performance lithium-sulphur batteries.* Electrochimica Acta, 2016. **196**: p. 369-376.

[50] Zhang, J., P. Gu, J. Xu, H. Xue, and H. Pang, *High performance of electrochemical lithium storage batteries: ZnO-based nanomaterials for lithium-ion and lithium-sulfur batteries.* Nanoscale, 2016. **8**(44): p. 18578-18595.

[51] Zhang, Q., Y. Wang, Z.W. Seh, Z. Fu, R. Zhang, and Y. Cui, *Understanding the Anchoring Effect of Two-Dimensional Layered Materials for Lithium-Sulfur Batteries.* Nano Lett, 2015. **15**(6): p. 3780-6.

[52] Yu, M., A. Wang, F. Tian, H. Song, Y. Wang, C. Li, J.D. Hong, and G. Shi, *Dual-protection of a graphene-sulfur composite by a compact graphene skin and an atomic layer deposited oxide coating for a lithium-sulfur battery.* Nanoscale, 2015. **7**(12): p. 5292-8.

[53] Fang, R., S. Zhao, S. Pei, X. Qian, P.X. Hou, H.M. Cheng, C. Liu, and F. Li, *Toward More Reliable Lithium-Sulfur Batteries: An All-Graphene Cathode Structure.* ACS Nano, 2016. **10**(9): p. 8676-82.

[54] Kaiser, M.R., Z. Ma, X. Wang, F. Han, T. Gao, X. Fan, J.Z. Wang, H.K. Liu, S. Dou, and C. Wang, *Reverse Microemulsion Synthesis of Sulfur/Graphene Composite for Lithium/Sulfur Batteries.* ACS Nano, 2017. **11**(9): p. 9048-9056.

[55] Chen, Z., W. Ren, L. Gao, B. Liu, S. Pei, and H.M. Cheng, *Three-dimensional flexible and conductive interconnected graphene networks grown by chemical vapour deposition.* Nat Mater, 2011. **10**(6): p. 424-8.

[56] Yu, P., X. Zhao, Z. Huang, Y. Li, and Q. Zhang, *Free-standing three-dimensional graphene and polyaniline nanowire arrays hybrid foams for high-performance flexible and lightweight supercapacitors.* J. Mater. Chem. A, 2014. **2**(35): p. 14413-14420.

[57] Duan, J., S. Chen, M. Jaroniec, and S.Z. Qiao, *Porous C3N4 nanolayers@N-graphene films as catalyst electrodes for highly efficient hydrogen evolution.* ACS Nano, 2015. **9**(1): p. 931-40.

[58] Alfonso, R., J. Xiaoting, H. John, N. Daniel, S. Hyungbin, B. Vladimir, D. MildredS, and K. Jing, *Large Area, Few-Layer Graphene Films on Arbitrary Substrates by Chemical Vapor Deposition.* Nano Lett, 2008. **9**(1): p. 30-35.

[59] Calizo, I., I. Bejenari, M. Rahman, G. Liu, and A.A. Balandin, *Ultraviolet Raman microscopy of single and multilayer graphene.* Journal of Applied Physics, 2009. **106**(4): p. 043509.

[60] Bayle, M., N. Reckinger, A. Felten, P. Landois, O. Lancry, B. Dutertre, J.-F. Colomer, A.-A. Zahab, L. Henrard, J.-L. Sauvajol, and M. Paillet, *Determining the number of layers in few-layer graphene by combining Raman spectroscopy and optical contrast.* Journal of Raman Spectroscopy, 2018. **49**(1): p. 36-45.

[61] Gu, X., C.-j. Tong, C. Lai, J. Qiu, X. Huang, W. Yang, B. Wen, L.-m. Liu, Y. Hou, and S. Zhang, *A porous nitrogen and phosphorous dual doped graphene blocking layer for high performance Li–S batteries.* J. Mater. Chem. A, 2015. **3**(32): p. 16670-16678.

[62] Cao, J., C. Chen, Q. Zhao, N. Zhang, Q. Lu, X. Wang, Z. Niu, and J. Chen, *A Flexible Nanostructured Paper of a Reduced Graphene Oxide-Sulfur Composite for High-Performance Lithium-Sulfur Batteries with Unconventional Configurations.* Adv Mater, 2016. **28**(43): p. 9629-9636.

[63] Xiao, P., F. Bu, G. Yang, Y. Zhang, and Y. Xu, *Integration of Graphene, Nano Sulfur, and Conducting Polymer into Compact, Flexible Lithium-Sulfur Battery Cathodes with Ultrahigh Volumetric Capacity and Superior Cycling Stability for Foldable Devices.* Adv Mater, 2017. **29**(40): p. 1703324-8.

[64] Yan, H., M. Cheng, B. Zhong, and Y. Chen, *Three-dimensional nitrogen-doped graphene/sulfur composite for lithium-sulfur battery.* Ionics, 2016. **22**(11): p. 1999-2006.

[65] Li, Z., Z. Ma, Y. Wang, R. Chen, Z. Wu, and S. Wang, *LDHs derived nanoparticle-stacked metal nitride as interlayer for long-life lithium sulfur batteries.* Science Bulletin, 2018. **63**(3): p. 169-175.

[66] Zhou, G., S. Pei, L. Li, D.W. Wang, S. Wang, K. Huang, L.C. Yin, F. Li, and H.M. Cheng, *A graphene-pure-sulfur sandwich structure for ultrafast, long-life lithium-sulfur batteries.* Adv Mater, 2014. **26**(4): p. 625-31, 664.

[67] Xi, K., P.R. Kidambi, R. Chen, C. Gao, X. Peng, C. Ducati, S. Hofmann, and R.V. Kumar, *Binder free three-dimensional sulphur/few-layer graphene foam cathode with enhanced high-rate capability for rechargeable lithium sulphur batteries.* Nanoscale, 2014. **6**(11): p. 5746-53.

[68] Sun, W., X. Ou, X. Yue, Y. Yang, Z. Wang, D. Rooney, and K. Sun, *A simply effective double-coating cathode with MnO_2 nanosheets/graphene as functionalized interlayer for high performance lithium-sulfur batteries.* Electrochimica Acta, 2016. **207**: p. 198-206.

[69] Yao, H., K. Yan, W. Li, G. Zheng, D. Kong, Z.W. Seh, V.K. Narasimhan, Z. Liang, and Y. Cui, *Improved lithium–sulfur batteries with a conductive coating on the separator to prevent the accumulation of inactive S-related species at the cathode–separator interface.* Energy Environ. Sci., 2014. **7**(10): p. 3381-3390.

[70] Ma, G., Z. Wen, Q. Wang, C. Shen, P. Peng, J. Jin, and X. Wu, *Enhanced performance of lithium sulfur battery with self-assembly polypyrrole nanotube film as the functional interlayer.* Journal of Power Sources, 2015. **273**: p. 511-516.